Hindawi
Journal of Nanomaterials
Volume 2023, Article ID 3098452, 10 pages
https://doi.org/10.1155/2023/3098452

Research Article

Effect of Temperature Sintering on Grain Growth and Optical Properties of TiO_2 Nanoparticles

Moges Tsega Yihunie

Department of Physics, College of Science, Bahir Dar University, P.O. Box 79, Bahir Dar, Ethiopia

Correspondence should be addressed to Moges Tsega Yihunie; mogestsega@yahoo.com

Received 29 July 2022; Revised 12 February 2023; Accepted 14 February 2023; Published 11 April 2023

Academic Editor: Rajalakshmanan Eswaramoorthy

Titanium dioxide (TiO_2) nanoparticles were prepared by the sol–gel method and the structural, morphological, and optical properties were investigated at different sintering temperatures of 500, 600, 700, 800, and 900°C. A tetragonal structure of anatase, mixed (anatase–rutile), and rutile phases are observed in the X-ray diffraction (XRD) analysis. Pure anatase phase formation occurred at 500°C, whereas anatase-to-rutile phase transformation began at 600°C, and reaching complete conversion to rutile at 800°C. The average crystallite size increased from 23 to 34 nm for anatase and 38 to 62 nm for the rutile when sintering temperature increased from 500 to 900°C. The scanning electron microscope (SEM) result presented the increase of grain size (25–100 nm) with increasing the sintering temperature. The Fourier transform infrared (FTIR) spectra demonstrated the presence of TiO_2 vibrational bonds in all samples. The optical bandgaps of the sintered TiO_2 nanoparticles decreased with rising sintering temperature. Photoluminescence spectra exhibited three characteristic peaks centered at 380, 450, and 550 nm. The emission intensity increased with increasing the sintering temperature. The Mie analysis was also studied to calculate scattering cross-section, forward scattering, and asymmetry for different grain sizes. The results showed that by increasing the nanoparticle diameters, the peaks of all spectra are redshifted for larger grain sizes and cross-section peaks shift to high values. In this study, the sintering temperature is observed to have a strong influence on crystalline phase transformation, microstructure, and optical properties of TiO_2 nanoparticles. The TiO_2 sample sintered at 900°C shows the best result to be used as luminescent material due to the low optical bandgap energy.

1. Introduction

Titanium dioxide (TiO_2) is a cheap, nontoxic, and nonbiodegradable material possessing many unique physical, chemical, and optical properties. Recently, nanostructured TiO_2 has attracted considerable attention because of its potential application in photocatalysis, gas sensors, solar cells, and lithium-ion batteries [1–3]. TiO_2 occurs naturally in three different crystalline phases: anatase, rutile, and brookite. Anatase and rutile are tetragonal, whereas brookite belongs to the orthorhombic crystalline system [4]. Each crystalline phase has different bandgaps that consist of different oriented TiO_6 octahedral chains [5]. Under ambient conditions, rutile is thermodynamically stable, whereas anatase and brookite are thermodynamically metastable. The anatase phase of TiO_2 is more effective as photocatalyst under UV light than rutile and brookite. However, its large bandgap (~3.2 eV) does not enable it to absorb light in the visible region. In comparison, the rutile phase of the TiO_2 was employed majorly in areas that involve high-end optics and electronics because of its high dielectric constant [6].

Several methods have been used by researchers to synthesize TiO_2 nanoparticles such as chemical precipitation [7], combustion [8], sol–gel [9, 10], and hydrothermal methods [11]. Among these methods, the sol–gel method is a simple process to synthesis TiO_2 nanoparticles. The sol–gel synthesis provides high purity, homogeneity, and high control over morphology and crystalline phases [12]. Different parameters such as precursor type, initial solution, pH, and heating temperatures affect the sol–gel synthesized powders [13, 14]. The different phases of TiO_2 nanoparticles can be obtained or maintained by controlling their temperature

[15, 16]. The anatase-to-rutile phase transformation significantly depends on the annealing time and annealing temperature [17]. Annealing modifies the crystal structure and, hence, the microstructural and morphological properties of TiO_2 [18–20]. The sintering temperature also results in a change of micrograin structure, crystallinity, morphology, grain size, etc. [21–24]. Dhiflaoui et al. [25] synthesized pure rutile TiO_2 nanoparticles after heating at 850°C. On the other hand, Bakri et al. [26] suggested that anatase/rutile phase transformation occurred at temperature >900°C.

In recent years, there has been an increasing interest in the study of optical scattering and absorption of TiO_2 nanoparticles using theoretical simulations. Despite the large amount of work on the synthesis, experimental characterization, and property measurements of TiO_2 nanoparticles, the number of reports with theoretical simulations is still quite limited [27, 28]. When the size of the particles becomes smaller, novel optical characteristics emerge [29]. The Mie analysis is one of the related computational methods used for studying the optical scattering and absorption properties. The Mie theory has the advantage of being conceptually simple and has found wide applicability in explaining experimental results. Theoretical calculations for the scattering coefficients depending on nanoparticle size were made using Mie calculations [30, 31]. In this work, the influence of different sintering temperatures (500, 600, 700, 800, and 900°C) on the phase transformation, crystallite size, surface morphology, and optical properties of TiO_2 nanoparticles prepared by sol–gel method was studied. Moreover, the Mie analysis was studied for different particle sizes of nanoparticles and scattering cross-section, forward scattering, and asymmetry were calculated.

2. Experimental Methods

Nanosized TiO_2 powder was synthesized via a sol–gel method using tetra-*n*-butyl orthotitanate ($C_{16}H_{36}O_4Ti$) (Sigma–Aldrich) as the titanium precursor, ethylenediamine ($C_2H_8N_2$) (Sigma–Aldrich) as the catalyst, and ethanol (C_2H_5OH) (Sigma–Aldrich) and deionized water (H_2O) as the solvent. In a typical experiment, 10 ml of tetra-*n*-butyl orthotitanate was added dropwise into 40 ml of ethanol and stirred for 2 hr. Deionized water was added to the mixture followed by the addition of ethylenediamine under vigorous stirring. The solutions were placed in the fume hood to chill for about 3–4 days where the milky gel was obtained. The obtained gel samples were then sintered in a muffle furnace at 500, 600, 700, 800, and 900°C for 1 hr and naturally cooled down to the room temperature.

X-ray diffraction (XRD) patterns of TiO_2 were measured using Bruker D8 X-ray diffractometer with Cu Kα radiation ($\lambda = 1.5406$ Å), with scattering angle of 20°–80°. The surface morphology of the samples was obtained with a field-emission scanning electron microscope (FE-SEM) (ZU SSX-550, Shimadzu). An energy-dispersive X-ray spectroscopy (EDS) spectrum was obtained by attaching to a SEM for elemental analysis. Fourier transform infrared (FTIR) (PerkinElmer STA 600 model) spectrometer was used to examine the synthesized nanoparticle's functional group using KBr. The reflectance spectra of the TiO_2 nanoparticles were measured using a PerkinElmer Lambda 950 UV–Vis photospectrometer. Photoluminescence (PL) spectra of the samples were measured at room temperature by using a Cary Eclipse fluorescence spectrophotometer (model LS 55) with a built-in 150 W xenon lamp as the excitation source and a grating to select a suitable wavelength for excitation.

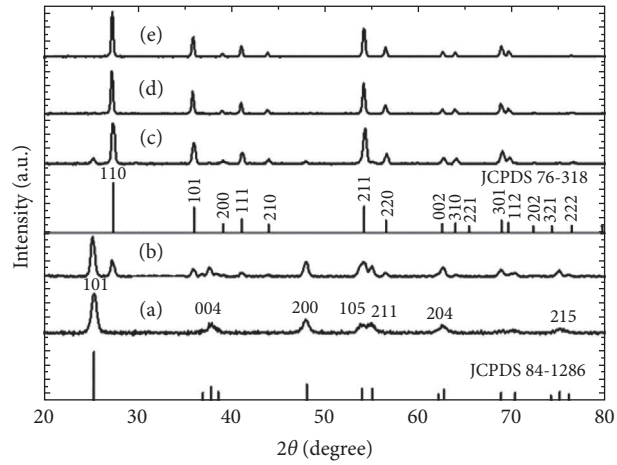

Figure 1: XRD patterns of TiO_2 nanoparticles sintered for 1 hr at (a) 500°C, (b) 600°C, (c) 700°C, (d) 800°C, and (e) 900°C.

3. Results and Discussion

Figure 1 shows the XRD patterns of the TiO_2 samples sintered at different temperatures (500, 600, 700, 800, and 900°C) for 1 hr. The sample sintered at 500°C was identified as nanocrystalline anatase phase and intense peak corresponding to (101) plane (Figure 1(a)). This phase formation is agreed with that obtained by Delekar et al. [32]. The major XRD diffraction peaks can be attributed to (101), (004), (200), (105), (211), (204), and (215) plane of anatase phase (JCPDS 84-1286) with tetragonal structure. More increased sintering temperature also causes phase transition from anatase to rutile. The rutile peaks appearing after sintering at 600°C indicate that phase transformation from anatase to rutile has occurred (Figure 1(b)). The rutile peaks become intense as the temperature increased to 700°C (Figure 1(c)). A complete transformation into rutile was occurred at 800°C (Figure 1(d)). Further increase to 900°C, the intensity of the (110) rutile orientation was also increased (Figure 1(e)) [15]. The rutile diffraction peaks correspond to the (110), (101), (200), (111), (210), (211), (220), (002), (310), and (301) tetragonal crystal planes which well matched with JCPDS file 76-318. Similar results have been reported in the literature [18, 33]. Arroyo et al. [34] reported that the transformation from anatase to rutile occurs above 800°C for pure TiO_2 materials. Zhang and Tang [35], however, reported that the complete transformation from anatase to rutile occurs above 900°C. It is noticed that intensity of the rutile diffraction peaks increases with increase in the sintering temperature, showing the degree of crystallinity of the nanopowders [36, 37].

Table 1: Anatase and rutile phase compositions and crystallite size of TiO_2 nanoparticles sintered at 500–900°C for 1 hr.

Calcined temperature (°C)	Crystal phase (%)		Crystallite size (nm)	
	Anatase	Rutile	Anatase	Rutile
500	100	–	23	–
600	78	22	31	38
700	14	86	34	42
800	–	100	–	49
900	–	100	–	62

The percentage of respective peaks corresponding to different phases is calculated by using the Spurr equation [38]:

$$R\,(\%) = \frac{I_{R(110)}}{0.884\, I_{A(101)} + I_{R(110)}} \times 100, \quad (1)$$

where I_A and I_R are peak intensities for (101) plane of anatase and (110) plane of rutile phases, respectively. The crystallite sizes (D) of the anatase and rutile phases are calculated by using the Scherrer equation [39]:

$$D = \frac{0.9\lambda}{\beta \cos\theta}, \quad (2)$$

where D is the crystallite size, λ is the X-ray wavelength, β is the full width at half maximum (FWHM) (in radian), and θ is the Bragg's diffraction angle. The average calculated crystallite size and phase composition of TiO_2 nanoparticles prepared at different sintering temperatures are presented in Table 1. At 600°C, the phase components were 78% for anatase and 22% for rutile. At 700°C, the percentages of anatase and rutile phases were also found to be 14% and 86%, respectively. Similar result has been reported in the literature [13]. A complete transformation from anatase to rutile phase was occurred at 800°C. It can be seen that with increasing sintering temperature to 700°C, the size of anatase phase crystallite increases from 23 to 34 nm. The crystallite size of rutile phase increased with increasing sintering temperature, with values of 38, 42, 49, and 62 nm at 600, 700, 800, and 900°C, respectively. The increase in crystallite size with increasing heating temperature may be attributed due to thermally promoted crystal growth. Anatase nanocrystallites having small size and high concentration of defects easily undergo phase transformation to rutile [40]. This result showed that the sintering temperature has a significant effect on the phase transformation, crystallite size, and crystallinity of TiO_2 nanoparticles.

Figure 2 shows the SEM image of TiO_2 nanoparticles sintered at 500, 600, 700, 800, and 900°C for 1 hr. Sample sintered at 500°C (Figure 2(a)) showed nonspherical small grains with a grain size of about 25 nm. As the sintering temperature increased to 600°C, the sizes became bigger with a grain size of about 35 nm, as shown in Figure 2(b). With increase in temperature to 700°C (Figure 2(c)), the sample showed well-defined near-spherical-shaped particles that are evolved into a clear and dense shape particle with grain sizes of about 50 nm. As further increase in temperature up to 800 (Figure 2(d)) and 900°C (Figure 2(e)), TiO_2 nanoparticles exhibited nonuniform shape of particles due to the agglomeration of initial particles with increase in grain size ranging from 80 to 100 nm. Grain boundaries can be clearly identified and a trend that the grain growth continued with the increase in the heating temperature was observed. Ostwald ripening at high temperatures leads to more nucleation of the nanoclusters and more growth [13, 17, 41]. Further, the sintering at 900°C (Figure 2(e)) showed large grain sizes of about 100 nm and showed a high degree of agglomeration [17]. The degree of agglomeration of TiO_2 nanoparticles is due to the adhesion of nanoparticles to each other and diffused boundaries [38, 42]. Moreover, the spherical morphology of the particles disappeared [17], indicating the crystal growth of titania with better densification. It is possible that some big particles with smooth interface embedded in the small crystallites forming large grains. At the highest calcination temperature, the particles and pores undergo melting-like process so that the coarsening rate for rutile will be significantly greater than that of anatase [43]. The increase in grain sizes due to aggregation of nanoparticles with the increased sintering temperature in the SEM patterns indicates increased crystallinity. The SEM results are in agreement with XRD results that showed the grain size of the anatase phase smaller than rutile phase due to aggregation of nanoparticles with increased sintering temperature. Similar results have been reported in other studies [17, 23, 44]. The histogram of particle size distribution of the TiO_2 nanoparticles sintered at 800 and 900°C was analyzed by using ImageJ software. The average grain size was estimated to be around 83 nm at 800°C (Figure 2(f)) and 90 nm at 900°C (Figure 2(g)). These values are close to the grain size estimated in the SEM images. It is clearly seen that the sintering temperature influences the morphology and size of the nanoparticles.

Figures 3(a) and 3(b) show the EDS spectrum of TiO_2 nanoparticles sintered at 800 and 900°C, respectively. The spectra have prominent peaks of titanium (Ti) and oxygen (O). No impurities were present. Atomic percentages of O decreased from 61.38 (51.52 wt%) to 56.18 (46.15 wt%) and Ti increased from 38.62 (48.48 wt%) to 43.82 (53.85 wt%), as the sintering temperature increased from 800 to 900°C. The O value is far below for the required theoretical atomic percentage of 66.67. The lower oxygen content could be attributed to the point defect in the form of oxygen vacancy in TiO_2 crystals at higher temperature.

Figure 4 shows the FTIR spectra of the sol–gel-driven TiO_2 nanoparticles sintered at 500–900°C for 1 hr. The bands around 3,401 and 2,959 cm^{-1} are assigned to the stretching vibrations of adsorbed water and hydrogen-bonded hydroxyl groups [45]. The broad peak observed at 2,425 cm^{-1} may correspond to the C–H stretching of hydrocarbon bonds. The bands at 2,050 and 1,950 cm^{-1} can be attributed to the vibrations of the C=O bonds in TiO_2 matrix. The peak at 1,650 cm^{-1} in the spectra is related to the stretching and bending vibrations of the Ti–OH and the –OH group of TiO_2 nanoparticles [41]. The absorption band observed in

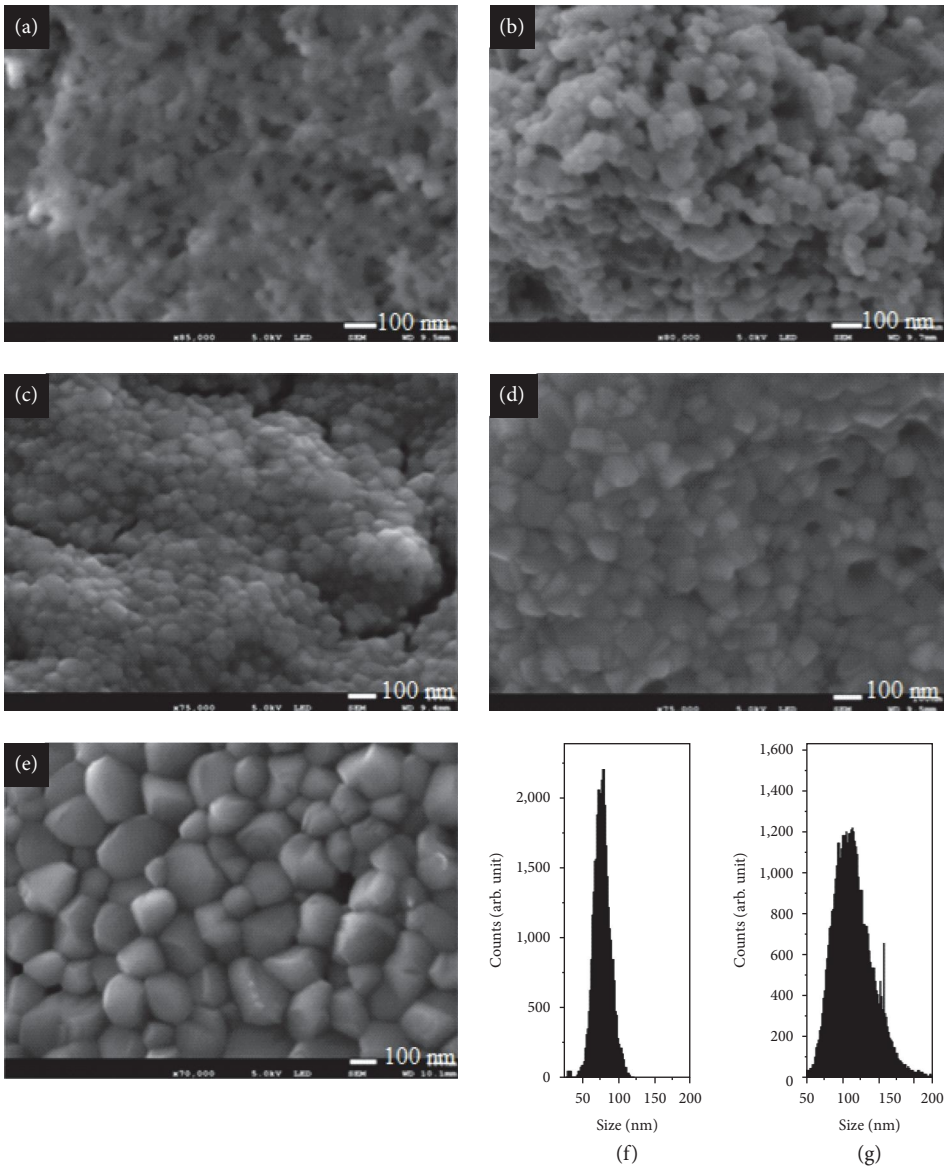

Figure 2: FE-SEM image of TiO_2 nanoparticles calcined at (a) 500°C, (b) 600°C, (c) 700°C, (d) 800°C, and (e) 900°C for 1 hr. Size distribution of TiO_2 nanoparticles sintered at (f) 800°C and (g) 900°C.

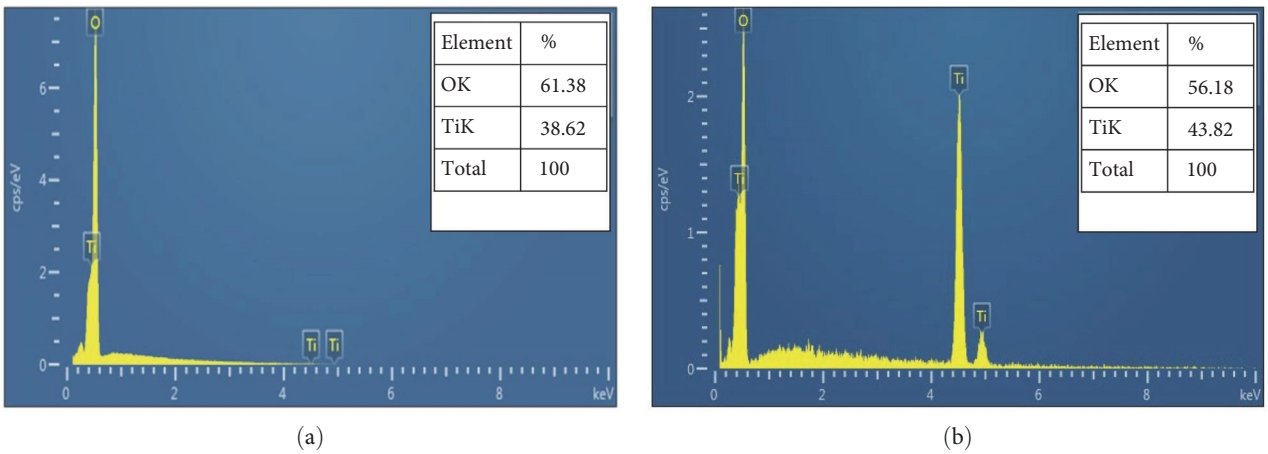

Figure 3: EDS analysis of TiO_2 nanoparticles sintered at (a) 800°C and (b) 900°C.

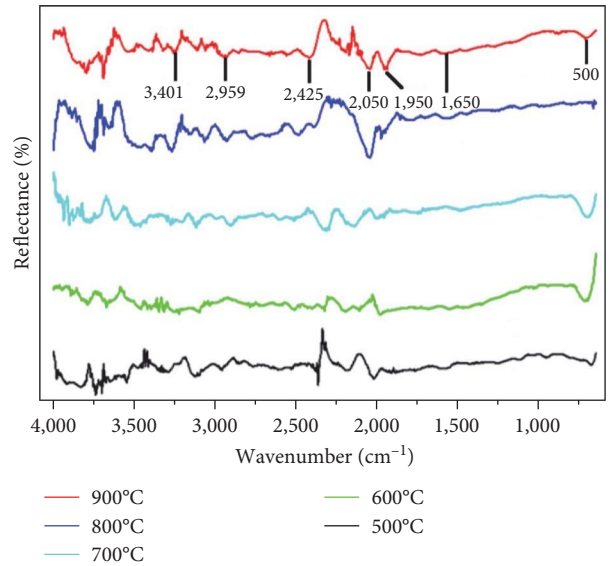

FIGURE 4: FTIR spectra of TiO_2 nanoparticles sintered at 500–900°C for 1 hr.

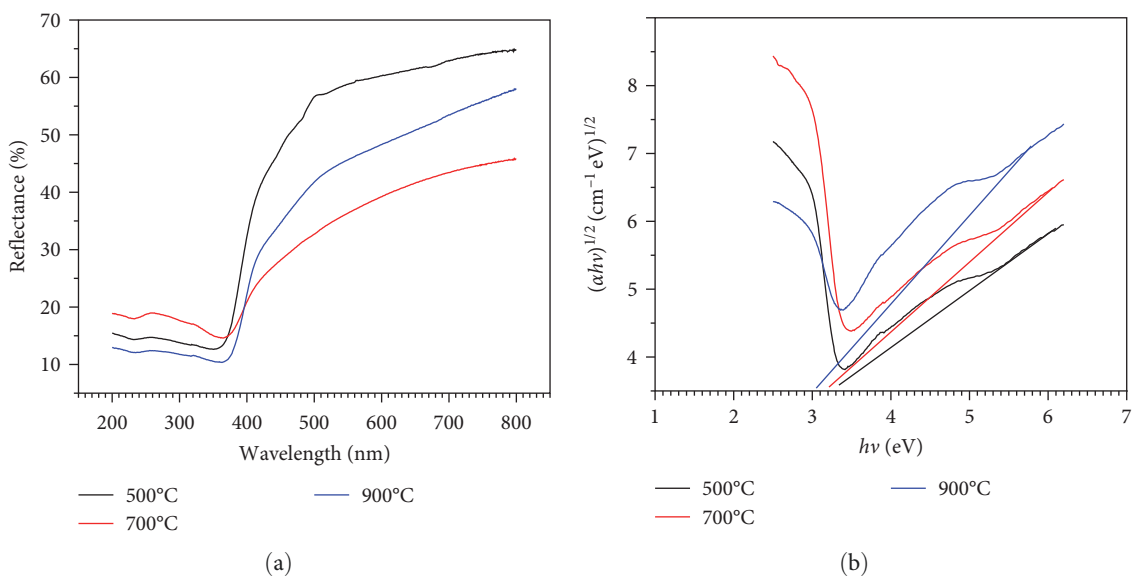

FIGURE 5: (a) UV–Vis reflectance spectra and (b) Tauc's plot of TiO_2 at different sintering temperatures.

the range of 400–800 cm^{-1} is the contribution from anatase titania. The peak at about 500 cm^{-1} can be attributed to the vibration of Ti–O bond in TiO_2 lattice [33, 46]. The absorption band at 730 cm^{-1} can be assigned to the Ti–O–Ti stretching vibrations [47]. The intensity of lower absorption bands decreased with the increase of the sintering temperature, indicating the removal of water molecules from the samples [48, 49]. For sintering above 800°C, additional intense absorption bands of exothermic peaks are observed. The exothermic peak can be associated with the crystallization of rutile TiO_2 [50]. Increase in sintering temperature results in the increase in crystallite size, thereby decreasing the surface area for adsorption of water.

The optical reflectance spectra of the as-prepared TiO_2 nanoparticles sintered at 500, 700, and 900°C were recorded at room temperature and shown in Figure 5(a). With the increase of sintering temperature, the absorption edge is observed to be shifted toward the higher wavelength with a redshift [51]. This is due to increase in crystallite size and the induced oxygen vacancy (defect sites) at higher sintering temperature. Figure 5(b) indicates bandgap plot calculated via Tauc equation for the corresponding samples. The reflectance

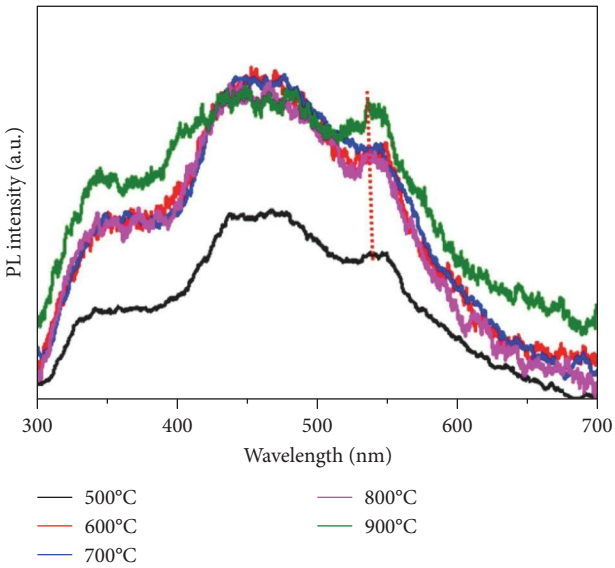

FIGURE 6: PL spectra of TiO_2 nanoparticles sintered at different temperatures.

data were converted to the absorption coefficient α values according to the Kubelka–Munk equation [52]:

$$\alpha = \frac{(1-R)^2}{2R}, \tag{3}$$

where α is the absorption coefficient and R is the reflectance. The absorption coefficient α and the bandgap E_g are related through the Tauc equation [53]:

$$(\alpha h\nu)^n = A\left(h\nu - E_g\right), \tag{4}$$

where $h\nu$ is the photon energy, A is a proportionality constant, and $n = 1/2$ is indirect bandgap transition. The optical bandgap energy can be calculated by plotting the graph of $(\alpha h\nu)^{1/2}$ vs. $h\nu$ and extrapolating the linear section of the curve to the $h\nu$ axis. The calculated bandgap values are 3.3, 3.2, and 3.1 eV corresponding to the samples sintered at temperature of 500, 700, and 900°C, respectively. The bandgap obtained at 500°C is larger than the bandgap of rutile TiO_2 sintered at 900°C. This trend is due to the phase transformation from anatase to rutile as clearly evident from XRD pattern [46]. At higher sintering temperature, growth of favored particles and agglomerates correspond to decrease in bandgap energy. This can be accounted as a result of increase in size of the crystallites by agglomeration at higher temperature [15, 24]. Hence, the reduced bandgap energies at raised sintering temperatures confirm the increase in grains as observed in SEM images. The narrowing of bandgap is prescribed to generation of new energy states in forbidden energy band of TiO_2 supporting photogeneration [54]. Similar results have been reported [15, 33].

Figure 6 shows the room temperature photoluminescence (PL) spectra of the sintered TiO_2 samples at 500, 600, 700, 800, and 900°C for 1 hr when excited at 320 nm. The PL peak positions that observed for anatase and rutile samples are similar, but relative intensities of these peaks are different. All samples exhibited broad emission peaks near 340–550 nm centered at 380, 470, and 550 nm. The observed broad and intense emission peaks originate from the recombination of exciton. The sample sintered at 500°C possesses the lowest PL intensity, revealing that the photogenerated holes and electrons have the lowest recombination rate in the sample. Samples sintered above 500°C induced an increase in the emission peaks. The UV emission band at 380 nm can be attributed to the indirect band-to-band transition from conduction band to valence band of TiO_2 nanoparticles [55]. The peaks observed at 470 and 550 nm are due to the self-trapped excitons, oxygen vacancies, and surface defects of TiO_2 [19, 56]. The PL intensity is a direct indicator for the charge recombination rate, i.e., stronger the PL intensity, higher the recombination rate and vice versa. The PL emission from sample sintered at 900°C is higher compared to the sample sintered at 500°C. Moreover, the increase in PL intensity for samples sintered at 600, 700, 800, and 900°C indicates the presence of mixed phases of anatase–rutile and pure rutile. This is also correlated that the increase in sintering temperature leads to the increase in the size of TiO_2 nanoparticles as observed in XRD and SEM investigations. By comparing the PL spectra of the TiO_2 samples sintered at 600, 700, and 800°C with that of the TiO_2 samples sintered at 900°C, it is clearly seen that the defect-related emission band at 530 nm is largely enhanced, while the blue emission at 470 nm is slightly suppressed. This can be attributed to the aggregation and rutile phase formation at elevated temperature, leading to an increased recombination process. At high sintering temperature, most of the nonradiative centers are covered up; however, thermally generated radiative oxygen vacancies become dominant defects in the TiO_2 lattice [56–58].

The Mie theory was used to calculate the optical parameters like scattering cross-section (C_{sca}), backscattering (Q_{rad}), and asymmetry (g). All waves incident on a particle are either absorbed or scattered. The scattering cross-section of a particle is the amount of light scattered by the particle relative to the light intercepted by its physical cross-section. The Mie solution, according to Maxwell's equations [59], describes the scattering of a plane wave by a particle and is given by:

$$\begin{aligned} C_{ext} &= \frac{2\pi}{k^2}\sum_{n=1}^{\infty}(2n+1)\mathrm{Re}(a_n + b_n), \\ C_{sca} &= \frac{2\pi}{k^2}\sum_{n=1}^{\infty}(2n+1)\{|a_n|^2 + |b_n|^2\}, \\ C_{abs} &= C_{ext} - C_{sca}, \end{aligned} \tag{5}$$

where $k = 2\pi/\lambda$ is the wavenumber and a_n and b_n are the Mie coefficients. Furthermore, the asymmetry parameter g indicates the average cosine of the scattering angle θ with respect to incident wavelength and is given by:

$$g = \langle \cos\theta \rangle. \tag{6}$$

Assuming that the index of refraction of TiO_2 is $n = 2.5$ and the incident radiation is $\lambda = 320$ nm. Theoretical

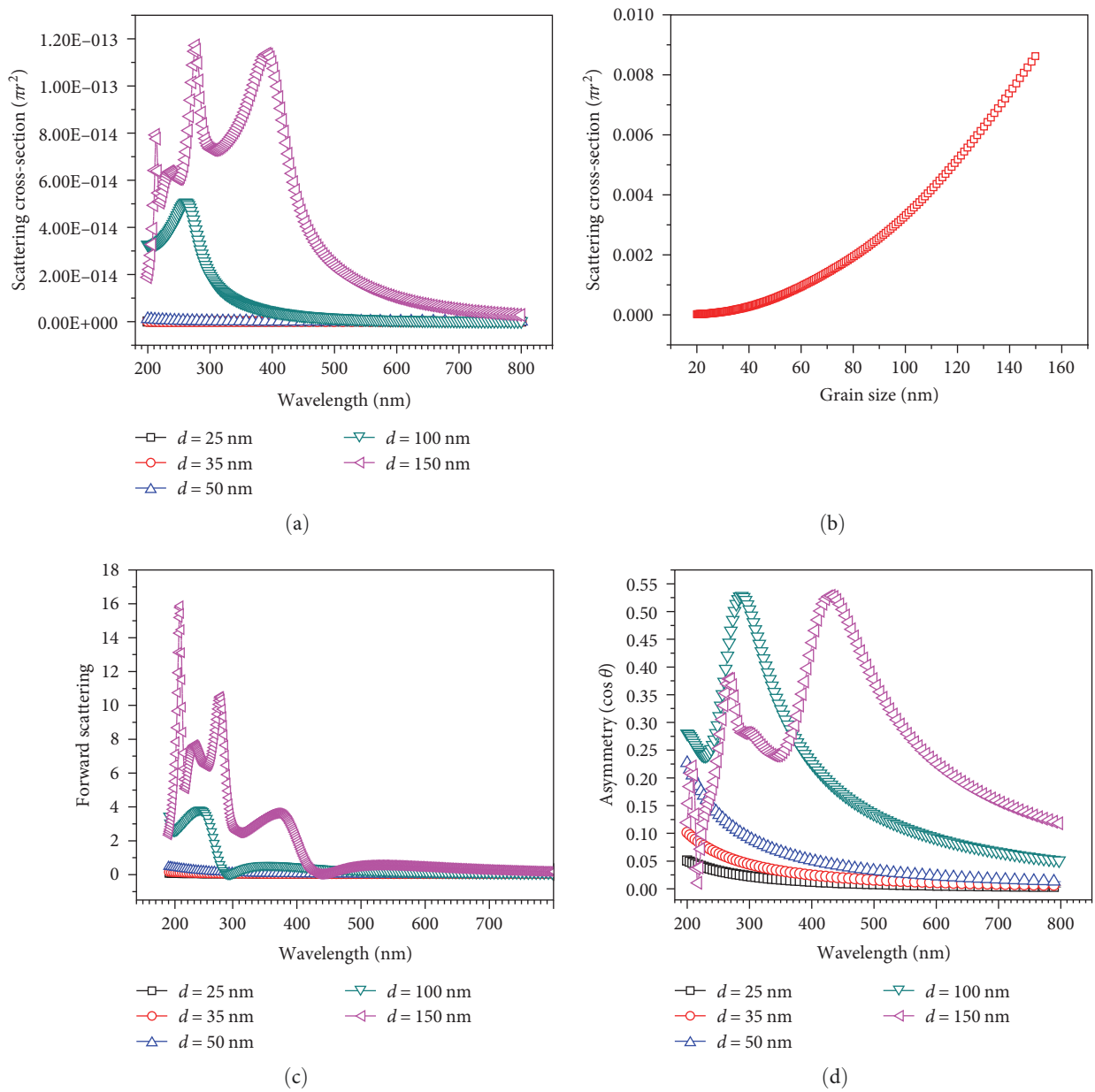

FIGURE 7: (a and b) The scattering cross-section, (c) forward scattering, and (d) asymmetry parameter of TiO_2 nanoparticles with varying grain sizes.

assessments of the scattering peak depending on nanoparticle size were made using Mie calculations, performed with software "Mie Plot v.4.3." Figure 7(a) shows the scattering cross-section of TiO_2 nanoparticles at different grain sizes (diameter = 25, 35, 50, 100, and 150 nm). It can be seen that the scattering cross-section peak is increased with increasing grain sizes, as shown in Figure 7(b). The numerical results showed that the scattering properties of nanoparticles with small particles vary smoothly with wavelength, while the scattering properties of nanoparticles with large particles oscillate with wavelength due to diffraction peaks. Moreover, the peak of all spectra is redshifted for larger particles. A redshifting of the scattering peak is expected for interparticle spacing of the order of the particle diameter [60]. Figure 7(c) shows the forward scattering of TiO_2 nanoparticles at the grain size of 25–150 nm. For nanoparticles with small grain sizes (25–50 nm), the forward scattering is increased slowly. However, the forward scattering is increased rapidly with the increase in grain size from 100 to 150 nm. For particles of 100 nm, an increase in the forward scattering is clearly visible, thus the scattering is asymmetric. With increasing particle size, the forward scattering becomes more pronounced, causing a larger asymmetry parameter, as shown in Figure 7(d). This is in agreement with the behavior of nonabsorbing systems [29].

4. Conclusion

Nanocrystalline TiO_2 particles were prepared by the sol–gel method sintered at 500, 600, 700, 800, and 900°C for 1 hr.

The XRD results showed that only tetragonal anatase phase is achieved at 500°C. A phase change occurs from anatase to mixed (anatase–rutile) to rutile with varying sintering temperatures. At 600°C, the phase transition from anatase to anatase–rutile mixed phase is noticed. The transformation from mixed phase to pure rutile was completed at 800°C. The average crystallite size of TiO_2 nanoparticles sintered at 500–900°C is found to lie in the range of 23–34 nm for anatase phase and 38–62 nm for rutile phase. The SEM results revealed an increase in grain size from 25 to 100 nm with increasing the calcination temperature from 500 to 900°C. At 900°C, the sample showed a bigger grain size of about 100 nm with clear grain structure and better densification. The stretching vibrational mode corresponds to anatase and rutile phases is explained by FTIR spectra of TiO_2 nanoparticles. From UV–Vis analysis, the bandgap of TiO_2 decreased from 3.3 to 3.1 eV with increasing sintering temperature from 500 to 900°C. The optical reflection study reveals that the reflection band edge shifts toward longer wavelength with increase of sintering temperature. The PL analysis shows the existence of both UV and visible emissions. A broad PL emission band from 350 to 550 nm is seen in all samples. Three characteristic peaks centered at 380, 450, and 550 nm were found. Further, PL spectroscopy revealed the change in emission intensity with sintering temperature and is in accordance with indirect transition. These defect-related emissions can be associated with the enhanced formation of surface defects and oxygen vacancies in the TiO_2 structure. The Mie analysis was studied and TiO_2 nanoparticles with different diameters were considered to investigate the correlation between the grain size and optical cross-section values. The results showed that by increasing the nanoparticle diameters, the peaks of all spectra are redshifted for larger grain sizes and cross-section peaks shift to high values. In this study, the sintering temperature is observed to be a key factor for the tuning of TiO_2 crystallite size, bandgap, and the phase transition.

Data Availability

The underlying data supporting the results of this study are found in the results and discussion part.

Additional Points

Highlights. Sol–gel-derived TiO_2 nanoparticles are studied for their phase transformation. The melting-like process accelerates the phase transition from anatase to rutile. The optical bandgaps of the sintered TiO_2 nanoparticles decreased with rising sintering temperature. The PL intensity and grain size increased with increasing sintering temperature. Redshifted and high scattering values for larger grain sizes were calculated. The suitability of Mie theory was estimated with scattering parameters.

Conflicts of Interest

The author declares that there is no conflicts of interest.

Funding

The authors acknowledge the financial support by the University of the Free State, Tertiary Education Support Program (ESKOM), and Organization of Protection of the Chemical Weapon (OPCW).

References

[1] C.-S. Chou, C.-Y. Chen, S.-H. Lin, W.-H. Lu, and P. Wu, "Preparation of TiO_2/bamboo-charcoal-powder composite particles and their applications in dye-sensitized solar cells," *Advanced Powder Technology*, vol. 26, no. 3, pp. 711–717, 2015.

[2] L. Huang, T. Liu, H. Zhang, W. W. Guo, and W. Zeng, "Hydrothermal synthesis of different TiO_2 nanostructures: structure, growth and gas sensor properties," *Journal of Materials Science: Materials in Electronics*, vol. 23, pp. 2024–2029, 2012.

[3] M. Zukalova, J. Prochazka, Z. Bastl et al., "Facile conversion of electrospun TiO_2 into titanium nitride/oxynitride fibers," *Chemistry of Materials*, vol. 22, no. 13, pp. 4045–4055, 2010.

[4] S. M. Gupta and M. Tripathi, "A review of TiO_2 nanoparticles," *Chinese Science Bulletin*, vol. 56, pp. 1639–1657, 2011.

[5] N. Tomić, M. Grujić-Brojčin, N. Finčur et al., "Photocatalytic degradation of alprazolam in water suspension of brookite type TiO_2 nanopowders prepared using hydrothermal route," *Materials Chemistry and Physics*, vol. 163, pp. 518–528, 2015.

[6] H. Cheng and A. Selloni, "Surface and subsurface oxygen vacancies in anatase TiO_2 and differences with rutile," *Physical Review B*, vol. 79, no. 9, Article ID 092101, 2009.

[7] L. Kernazhitsky, V. Shymanovska, V. Naumov et al., "Room temperature photoluminescence of mixed titanium–manganese oxides," *Journal of Luminescence*, vol. 187, pp. 521–527, 2017.

[8] J. Shi and X. Wang, "Growth of rutile titanium dioxide nanowires by pulsed chemical vapor deposition," *Crystal Growth & Design*, vol. 11, no. 4, pp. 949–954, 2011.

[9] M. Aqeel, M. Ikram, M. Imran et al., "TiO_2 Co-doped with Zr and Ag shows highly efficient visible light photocatalytic behaviour suitable for treatment of polluted water," *RCS Advances*, vol. 10, no. 69, pp. 42235–42248, 2020.

[10] M. Ikram, J. Hassan, A. Raza et al., "Photocatalytic and bactericidal properties and molecular docking analysis of TiO_2 nanoparticles conjugated with Zr for environmental remediation," *RCS Advances*, vol. 10, no. 50, pp. 30007–30024, 2020.

[11] K. A. Malinger, A. Maguer, A. Thorel, A. Gaunand, and J.-F. Hochepied, "Crystallization of anatase nanoparticles from amorphous precipitate by a continuous hydrothermal process," *Chemical Engineering Journal*, vol. 174, no. 1, pp. 445–451, 2011.

[12] K. Namratha and K. Byrappa, "Novel solution routes of synthesis of metal oxide and hybrid metal oxide nanocrystals," *Progress in Crystal Growth and Characterization of Materials*, vol. 58, no. 1, pp. 14–42, 2012.

[13] B. K. Mutuma, G. N. Shao, W. D. Kim, and H. T. Kim, "Sol–gel synthesis of mesoporous anatase–brookite and anatase–brookite–rutile TiO_2 nanoparticles and their photocatalytic properties," *Journal of Colloid and Interface Science*, vol. 442, pp. 1–7, 2015.

[14] L. Agartan, D. Kapusuz, J. Park, and A. Ozturk, "Effect of initial water content and calcination temperature on photocatalytic properties of TiO_2 nanopowders synthesized by the sol–gel process," *Ceramics International*, vol. 41, no. 10, pp. 12788–12797, 2015.

[15] R. S. Dubey, "Temperature-dependent phase transformation of TiO_2 nanoparticles synthesized by sol–gel method," *Materials Letters*, vol. 215, pp. 312–317, 2018.

[16] S. Sugapriya, R. Sriram, and S. Lakshmi, "Effect of annealing on TiO_2 nanoparticles," *Optik*, vol. 124, no. 21, pp. 4971–4975, 2013.

[17] C. R. Tubío, F. Guitián, J. R. Salgueiro, and A. Gil, "Anatase and rutile TiO_2 monodisperse microspheres by rapid thermal annealing: a method to avoid sintering at high temperatures," *Materials Letters*, vol. 141, pp. 203–206, 2015.

[18] D. S. Kim, S. J. Han, and S.-Y. Kwak, "Synthesis and photocatalytic activity of mesoporous TiO_2 with the surface area, crystallite size, and pore size," *Journal of Colloid and Interface Science*, vol. 316, no. 1, pp. 85–91, 2007.

[19] L. Kernazhitsky, V. Shymanovska, T. Gavrilko et al., "Room temperature photoluminescence of anatase and rutile TiO_2 powders," *Journal of Luminescence*, vol. 146, pp. 199–204, 2014.

[20] L. Yu, X. Yang, J. He, Y. He, and D. Wang, "One-step hydrothermal method to prepare nitrogen and lanthanum co-doped TiO_2 nanocrystals with exposed {001} facets and study on their photocatalytic activities in visible light," *Journal of Alloys and Compounds*, vol. 637, pp. 308–314, 2015.

[21] L. Kadri, G. Bulai, A. Carlescu et al., "Effect of target sintering temperature on the morphological and optical properties of pulsed laser deposited TiO_2 thin films," *Coatings*, vol. 11, no. 5, Article ID 561, 2021.

[22] M. K. Hossain, M. F. Pervez, M. N. H. Mia et al., "Annealing temperature effect on structural, morphological and optical parameters of mesoporous TiO_2 film photoanode for dye-sensitized solar cell application," *Materials Science-Poland*, vol. 35, no. 4, pp. 868–877, 2017.

[23] S. Chao, V. Petrovsky, and F. Dogan, "Effects of sintering temperature on the microstructure and dielectric properties of titanium dioxide ceramics," *Journal of Materials Science*, vol. 45, pp. 6685–6693, 2010.

[24] M. C. Mathpal, A. K. Tripathi, M. K. Singh, S. P. Gairola, S. N. Pandey, and A. Agarwal, "Effect of annealing temperature on Raman spectra of TiO_2 nanoparticles," *Chemical Physics Letters*, vol. 555, pp. 182–186, 2013.

[25] H. Dhiflaoui, N. B. Jaber, F. S. Lazar, J. Faure, A. B. C. Larbi, and H. Benhayoune, "Effect of annealing temperature on the structural and mechanical properties of coatings prepared by electrophoretic deposition of TiO_2 nanoparticles," *Thin Solid Films*, vol. 638, pp. 201–212, 2017.

[26] A. S. Bakri, M. Z. Sahdan, F. Adriyanto et al., "Effect of annealing temperature of titanium dioxide thin films on structural and electrical properties," *AIP Conference Proceedings*, vol. 1788, no. 1, Article ID 030030, 2017.

[27] H. Bech and A. Leder, "Simultaneous determination of particle size and refractive index by time-resolved Mie scattering," *Optik*, vol. 121, no. 20, pp. 1815–1823, 2010.

[28] A. Rastar, M. E. Yazdanshenas, A. Rashidi, and S. M. Bidoki, "Estimation and prediction of optical properties of PA6/TiO_2 nanocomposites," *Arabian Journal of Chemistry*, vol. 10, Suppl 1, pp. S219–S224, 2017.

[29] H. Akherat Doost, M. H. Majles Ara, and E. Koushki, "Synthesis and complete Mie analysis of different sizes of TiO_2 nanoparticles," *Optik*, vol. 127, no. 4, pp. 1946–1951, 2016.

[30] I. Niskanen, V. Forsberg, D. Zakrisson et al., "Determination of nanoparticle size using Rayleigh approximation and Mie theory," *Chemical Engineering Science*, vol. 201, pp. 222–229, 2019.

[31] J. R. Dunklin, G. T. Forcherio, and D. Keith Roper, "Gold nanoparticle-polydimethylsiloxane films reflect light internally by optical diffraction and Mie scattering," *Materials Research Express*, vol. 2, no. 8, Article ID 085005, 2015.

[32] S. D. Delekar, H. M. Yadav, S. N. Achary, S. S. Meena, and S. H. Pawar, "Structural refinement and photocatalytic activity of Fe-doped anatase TiO_2 nanoparticles," *Applied Surface Science*, vol. 263, pp. 536–545, 2012.

[33] M. Lal, P. Sharma, and C. Ram, "Calcination temperature effect on titanium oxide (TiO_2) nanoparticles synthesis," *Optik*, vol. 241, Article ID 166934, 2021.

[34] R. Arroyo, G. Córdoba, J. Padilla, and V. H. Lara, "Influence of manganese ions on the anatase–rutile phase transition of TiO_2 prepared by the sol–gel process," *Materials Letters*, vol. 54, no. 5-6, pp. 397–402, 2002.

[35] W. Zhang and H. Tang, "Rutile nanopowders for pigment production: formation mechanism and particle size prediction," *Chemical Physics Letters*, vol. 692, pp. 129–133, 2018.

[36] Y. Rambabu, M. Jaiswal, and S. C. Roy, "Effect of annealing temperature on the phase transition, structural stability and photo-electrochemical performance of TiO_2 multi-leg nanotubes," *Catalysis Today*, vol. 278, Part 2, pp. 255–261, 2016.

[37] V. T. Lukong, K. O. Ukoba, and T. C. Jen, "Heat-assisted sol–gel synthesis of TiO_2 nanoparticles structural, morphological and optical analysis for self-cleaning application," *Journal of King Saud University - Science*, vol. 34, no. 1, Article ID 101746, 2022.

[38] R. A. Spurr and H. Myers, "Quantitative analysis of anatase-rutile mixtures with an X-ray diffractometer," *Analytical Chemistry*, vol. 29, no. 5, pp. 760–762, 1957.

[39] A. L. Patterson, "The Scherrer formula for X-ray particle size determination," *Physical Review*, vol. 56, no. 10, pp. 978–982, 1939.

[40] D. Li, X. Cheng, X. Yu, and Z. Xing, "Preparation and characterization of TiO_2-based nanosheets for photocatalytic degradation of acetylsalicylic acid: influence of calcination temperature," *Chemical Engineering Journal*, vol. 279, pp. 994–1003, 2015.

[41] N. Rathore, A. Kulshreshtha, R. K. Shukla, and D. Sharma, "Study on morphological, structural and dielectric properties of sol–gel derived TiO_2 nanocrystals annealed at different temperatures," *Physica B: Condensed Matter*, vol. 582, Article ID 411969, 2020.

[42] S. Saravanan and R. S. Dubey, "Optical and morphological studies of TiO_2 nanoparticles prepared by sol–gel method," *Materials Today: Proceedings*, vol. 47, Part 9, pp. 1811–1814, 2021.

[43] H. Shi, D. Zeng, J. Li, and W. Wang, "A melting-like process and the local structures during the anatase-to-rutile transition," *Materials Characterization*, vol. 146, pp. 237–242, 2018.

[44] N. Yuangpho, S. T. T. Le, T. Treerujiraphapong, W. Khanitchaidecha, and A. Nakaruk, "Enhanced photocatalytic performance of TiO_2 particles via effect of anatase–rutile ratio," *Physica E: Low-Dimensional Systems and Nanostructures*, vol. 67, pp. 18–22, 2015.

[45] Z. He, W. Que, J. Chen, Y. He, and G. Wang, "Surface chemical analysis on the carbon-doped mesoporous TiO_2 photocatalysts after post-thermal treatment: XPS and FTIR characterization," *Journal of Physics and Chemistry of Solids*, vol. 74, no. 7, pp. 924–928, 2013.

[46] P. Shah, N. Agrawal, N. Reddy Ravuru, and S. Patel, "Ultrafine titanium-dioxide (rutile) based nano-crystalline dispersions as a pigment for waterborne coatings," *Progress in Color, Colorants and Coatings*, vol. 15, no. 4, pp. 305–318, 2022.

[47] P. Praveen, G. Viruthagiri, S. Mugundan, and N. Shanmugam, "Structural, optical and morphological analyses of pristine titaniu di-oxide nanoparticles–synthesized via sol–gel route," *Spectrochimica Acta Part A: Molecular and Biomolecular Spectroscopy*, vol. 117, pp. 622–629, 2014.

[48] M. S. Ghamsari, M. R. Gaeeni, W. Han, and H.-H. Park, "Highly stable colloidal TiO_2 nanocrystals with strong violet–blue emission," *Journal of Luminescence*, vol. 178, pp. 89–93, 2016.

[49] N. C. Horti, M. D. Kamatagi, N. R. Patil, S. K. Nataraj, M. S. Sannaikar, and S. R. Inamdar, "Synthesis and photoluminescence properties of titanium oxide (TiO_2) nanoparticles: effect of calcination temperature," *Optik*, vol. 194, Article ID 163070, 2019.

[50] Y. F. You, C. H. Xu, S. S. Xu et al., "Structural characterization and optical property of TiO_2 powders prepared by the sol–gel method," *Ceramics International*, vol. 40, no. 6, pp. 8659–8666, 2014.

[51] M. K. Singh and M. S. Mehata, "Temperature-dependent photoluminescence and decay times of different phases of grown TiO_2 nanoparticles: carrier dynamics and trap states," *Ceramics International*, vol. 47, no. 23, pp. 32534–32544, 2021.

[52] E. L. Simmons, "Diffuse reflectance spectroscopy: a comparison of the theories," *Applied Optics*, vol. 14, no. 6, pp. 1380–1386, 1975.

[53] M. Sreemany and S. Sen, "A simple spectrophotometric method for determination of the optical constants and band gap energy of multiple layer TiO_2 thin films," *Materials Chemistry and Physics*, vol. 83, no. 1, pp. 169–177, 2004.

[54] Z. Noorimotlagh, I. Kazeminezhad, N. Jaafarzadeh, M. Ahmadi, Z. Ramezani, and S. Silva Martinez, "The visible-light photodegradation of nonylphenol in the presence of carbon-doped TiO_2 with rutile/anatase ratio coated on GAC: effect of parameters and degradation mechanism," *Journal of Hazardous Materials*, vol. 350, pp. 108–120, 2018.

[55] A. M. Selman, Z. Hassan, and M. Husham, "Structural and photoluminescence studies of rutile TiO_2 nanorods prepared by chemical bath deposition method on Si substrates at different pH values," *Measurement*, vol. 56, pp. 155–162, 2014.

[56] S. A. Ahmed, "Annealing effects on structure and magnetic properties of Mn-doped TiO_2," *Journal of Magnetism and Magnetic Materials*, vol. 402, pp. 178–183, 2016.

[57] K. P. Ghoderao, S. N. Jamble, and R. B. Kal, "Influence of reaction temperature on hydrothermally grown TiO_2 nanorods and their performance in dye-sensitized solar cells," *Superlattices Microstructures*, vol. 124, pp. 121–130, 2018.

[58] M. Tsega and F. B. Dejene, "Morphological, thermal and optical properties of TiO_2 nanoparticles: the effect of titania precursor," *Materials Research Express*, vol. 6, no. 6, Article ID 065041, 2019.

[59] W. J. Wiscombe, "Improved Mie scattering algorithms," *Applied Optics*, vol. 19, no. 9, pp. 1505–1509, 1980.

[60] J. Tan, Y. Xie, F. Wang, L. Jing, and L. Ma, "Investigation of optical properties and radiative transfer of TiO_2 nanofluids with the consideration of scattering effects," *International Journal of Heat and Mass Transfer*, vol. 115, pp. 1103–1112, 2017.